Revision 1

Title: High-pressure synthesis of skiagite-majorite garnet and investigation of its crystal structure

Authors and affiliation:

Leyla Ismailova[1,2], Andrey Bobrov[3], Maxim Bykov[1], Elena Bykova[1,2], Valerio Cerantola [2], Innokenty Kantor[4], Ilya Kupenko[4], Catherine McCammon[2], Vadim Dyadkin[4], Dmitry Chernyshov[4], Sakura Pascarelli[4], Alexander Chumakov[4], Natalia Dubrovinskaia[1], Leonid Dubrovinsky[2]

[1] Laboratory of Crystallography, Universität Bayreuth, 95447 Bayreuth, Germany

[2] Bayerisches Geoinstitut, Universität Bayreuth, 95447 Bayreuth, Germany

[3] Department of Petrology, Geological Faculty, Moscow State University, 119234 Moscow, Russia

[4] ESRF – European Synchrotron Radiation Facility, CS40220 38043 Grenoble Cedex 9, France

Corresponding Author: Leyla Ismailova, M.Sc leyla.isml@gmail.com

Abstract:

Skiagite-rich garnet was synthesized as single crystals at 9.5 GPa and 1100 °C using a multi-anvil apparatus. The crystal structure (cubic, space group $Ia\bar{3}d$, a=11.7511(2) Å, V=1622.69(5) Å^3 , D_{calc}=4.4931 g/cm^3) was investigated using single crystal synchrotron X-ray diffraction. Synchrotron Mössbauer Source spectroscopy revealed that Fe^{2+} and Fe^{3+} predominantly occupy dodecahedral (X) and octahedral (Y) sites, respectively, as expected for the garnet structure, and confirmed independently using nuclear forward scattering. Single-crystal X-ray diffraction suggests the structural formula of the skiagite-rich garnet to

be $Fe^{2+}_3(Fe^{2+}_{0.234(2)}Fe^{3+}_{1.532(1)}Si^{4+}_{0.234(2)})(SiO_4)_3$, in agreement with electron microprobe chemical analysis. The formula is consistent with X-ray absorption near-edge structure spectra. The occurrence of Si and Fe^{2+} in the octahedral Y-site indicates the synthesized garnet to be a solid solution of endmember skiagite with ~23 mol% of the Fe-majorite endmember $Fe^{2+}_3(Fe^{2+}Si^{4+})(SiO_4)_3$.

Keywords: skiagite, majorite, garnets, single crystal X-ray diffraction, Mossbauer spectroscopy, Nuclear forward scattering, XANES

Body of paper

Introduction

Garnet is a common mineral in mantle assemblages and often occurs as inclusions in natural diamonds. Due to the compositional complexity of natural garnets, the relationship between their composition and the pressure-temperature conditions of their formation is still not well constrained (Akaogi and Akimoto 1977; Irufune 1987; Stachel 2001; Collerson 2010).

Silicate garnets have the general formula $[X]_3[Y]_2Si_3O_{12}$ where [X] and [Y] are cations occupying the dodecahedral and octahedral sites, respectively. In garnets from the crust and upper mantle the dodecahedral site is occupied by a divalent cation (e.g., Fe^{2+}, Mg^{2+}, Ca^{2+}) and the octahedral site by a trivalent cation (e.g., Fe^{3+}, Al^{3+}, Cr^{3+}). Garnets from mantle xenoliths and inclusions in diamonds contain both ferrous (Fe^{2+}) and ferric (Fe^{3+}) iron. Thus information about the properties and high-pressure behaviour of the iron endmember skiagite, $Fe^{2+}_3Fe^{3+}_2(SiO_4)_3$, is important for mineral physics and the geochemistry of the Earth's upper mantle and transition zone. Moreover, the fate of iron-rich silicate material incorporating a

skiagite component is unknown at conditions of the deep lower mantle and the core-mantle boundary.

The stability field of skiagite has been investigated in several studies. Karpinskaya et al. (1982) were probably the first to synthesize skiagite, which was produced at 12 GPa and 800°C. Woodland and O'Neill (1993) measured the variation of garnet unit cell parameter along the almandine-skiagite solid solution join. Woodland and Ross (1994) studied the crystal chemistry of skiagite solid solutions along the joins $Fe_3Al_2(SiO_4)_3$ – $Fe_3Fe_2(SiO_4)_3$ (almandine-skiagite) and $Ca_3Fe_2(SiO_4)_3$ – $Fe_3Fe_2(SiO_4)_3$ (andradite-skiagite) at pressures between 1.7 and 9.7 GPa and temperatures of 1080 to1100 °C. Woodland and O'Neill (1995) investigated the stability of Ca-bearing garnets on the join $Ca_3Fe_2(SiO_4)_3$ – $Fe_3Fe_2(SiO_4)_3$ (andradite-skiagite) as a function of pressure at 1100 °C. Simple Cr^{3+}-Fe^{3+} exchange in the octahedral sites of the skiagite – Fe-knorringite ($Fe_3Fe_2(SiO_4)_3$-$Fe_3Cr_2(SiO_4)_3$) binary join was studied by Woodland et al. (2009). However, so far the iron-skiagite endmember has not yet been synthesized so that it can be investigated by mineral physics methods, including single crystal X-ray diffraction and Mössbauer spectroscopy.

Here we report the high-pressure high-temperature synthesis of single crystals of skiagite-rich garnet, $Fe^{2+}_3(Fe^{2+}_{0.234(2)}Fe^{3+}_{1.53(1)}Si_{0.234(2)})(SiO_4)_3$, and the results of its characterization using single-crystal synchrotron X-ray diffraction, synchrotron Mössbauer source (SMS) spectroscopy, nuclear forward scattering (NFS), and X-ray absorption near-edge structure (XANES) spectroscopies .

Experimental methods

Synthesis experiments were performed using a split-sphere type multi-anvil apparatus at 9.5 GPa and 1100° C at Bayerisches Geoinstitut (Bayreuth, Germany) (BGI). The starting material (corresponding to the nominal composition $Fe_3Fe_2Si_3O_{12}$) was a powdered mixture of

chemically pure oxides ($Fe_{1-x}O$, $^{57}Fe_2O_3$ and SiO_2) homogenized at room temperature by milling in a mortar using ethanol and then dried in a furnace at 100 °C for 24 hours. The prepared mixture was placed in a capsule of 3.5 mm length and 2 mm diameter made of platinum foil. High temperature was generated using a $LaCrO_3$ heater and the capsule was insulated from the heater by a MgO cylinder. The cell assembly with the sample was compressed to the target pressure between eight cubic tungsten carbide anvils with corners truncated to 11.0 mm edge lengths. The accuracy in determination of pressure and temperature is estimated to be ±0.5 GPa and ±50 ^{o}C, respectively (Frost 2004). The sample was heated for about 30 min and rapidly quenched by switching off the power supply, causing cooling to ambient temperature with a rate of ~200 ^{o}C/s.

Chemical composition of the samples was characterized using wavelength dispersive X-ray (WDX) microprobe analysis (JEOL JXA-8200; focused beam; accelerating voltage of 15 keV and beam current of 15 nA). Metallic Fe and quartz were used as standards for Fe and Si, respectively, with atomic number effects, absorption, and fluorescence (ZAF) correction.

SMS spectra were recorded at the Nuclear Resonance Beamline (Rüffer and Chumakov 1996) ID18 of the European Synchrotron Radiation Facility (ESRF) (Grenoble, France) using the (111) Bragg reflection of a $^{57}FeBO_3$ single crystal mounted on a Wissel velocity transducer driven with a sinusoidal wave form (Potapkin et al. 2012). The X-ray beam was focused to 20 μm vertical and 10 μm horizontal dimensions using Kirkpatrick-Baez mirrors. The linewidth of the SMS and the absolute position of the center shift (CS) were controlled before and after each measurement using a $K_2Mg^{57}Fe(CN)_6$ reference single line absorber. The velocity scale was calibrated using 25 μm thick natural α-Fe foil. Each spectrum took ~ 1-2 hours to collect. Spectra were fitted using a full transmission integral with a normalized Lorentzian-squared source lineshape using the MossA software package (Prescher et al. 2012).

NFS data were collected at the same beamline in 4-bunch mode, with the beam focused to 6×11 μm^2 using Kirkpatrick-Baez mirrors. The spectra were collected for 10 to 60 min each. NFS data were fitted using the CONUSS package (Sturhahn 2000).

XANES spectra were collected at the energy-dispersive X-ray absorption spectroscopy beamline (ID24) at ESRF. The beam was focused horizontally using a curved polychromator Si (111) crystal in Bragg geometry and vertically with Kirkpatrick-Baez (KB) mirrors. The size of the X-ray beam spot on the sample was about 3.5 x 5 μm^2 FWHM. The measured XANES spectra were normalized using FDMNES software (Bunau and Joly 2009). The second-order polynomial pixel to energy conversion parameters were calibrated using a reference α-Fe foil. Crystals for all studies were selected at BGI using a three-circle Bruker diffractometer equipped with a SMART APEX CCD detector and a high-brilliance Rigaku diffractometer equipped with a rotating anode (Rotor Flex FR-D, Mo-Kα radiation), Osmic focusing X-ray optics, and Bruker Apex CCD detector.

Single crystal X-ray diffraction data were collected at the Swiss-Norwegian beamline (BM01A) at ESRF on a single-crystal diffractometer (KUMA KM6-CH) by 360° φ scans (Δφ = 0.5°) employing a Pilatus 2M pixel detector. The crystal was cooled to 280 K using an Oxford Cryostream low-temperature device. Data processing (peak intensity integration, background evaluation, cell parameters, space group determination and absorption correction) was performed with the *CrysAlis*^{Pro} 171.36.28 program. The program *JANA2006* was used for structure refinement (Petricek et al. 2014).

Results and discussion

Phase assemblage and chemical composition

The recovered sample is a multi-phase assemblage that includes fine anhedral garnet crystals that appear red under a light microscope and typically have dimensions less than 30x10x10 μm^3. There are also minor amounts of magnetite, coesite and clinopyroxene (Fig. 1) that were confirmed by X-ray diffraction data and microprobe analysis. The presence of other phases in addition to garnet may indicate a non-homogeneous pressure-temperature distribution within the pressure chamber and/or different kinetics of chemical reactions in the starting mixture.

The composition of skiagite garnet was obtained by averaging 30 microprobe analyses (in wt% with standard deviations given in parentheses): SiO_2 35.21(11), FeO 60.67(9), total 95.88(14), which led to a chemical formula of $Fe^{2+}_3(Fe^{2+}_{0.276(1)}Fe^{3+}_{1.44(1)}Si_{0.276(1)})Si_3O_{12}$ on the basis of 12 oxygen atoms assuming stoichiometry and that the dodecahedral position is occupied exclusively by Fe^{2+}. The Fe^{3+}-corrected values of the microprobe analyses are (in wt%): SiO_2 35.21(11), FeO 42.11 (36), Fe_2O_3 20.63 (80), total 97.95(88). No chemical zoning was observed in the run products. As evident from the formula, there is an excess of Si over the ideal 3 atoms per formula unit.

Single crystal X-ray diffraction and structure refinement

The experimental details and crystallographic data obtained by means of synchrotron X-ray diffraction from a small (red) crystal of skiagite garnet are summarized in Table 1. Fractional atomic coordinates and isotropic or equivalent isotropic displacement parameters ($Å^2$), atomic displacement parameters ($Å^2$), selected geometric parameters (Å, º) are listed in Tables 2–4. Full-matrix least-squares refinement on *F* provided good reliability factors $R_F(I>3\sigma(I)) = 0.0281$ and $wR_F(\text{all}) = 0.0427$. Atomic coordinates and anisotropic displacement

parameters of Fe1 and Si1 were constrained to be equal, and their overall occupancy was fixed. Structure refinement revealed that the octahedral site is fully occupied by Fe and Si atoms, yielding the chemical composition $Fe^{2+}_3(Fe^{2+}_{0.234(2)}Fe^{3+}_{1.532(1)}Si^{4+}_{0.234(2)})(SiO_4)_3$, which is in good agreement with the results of electron microprobe analysis. The minor difference in the chemical composition determined by these two methods is likely due to the bulk averaging of the microprobe data compared to the diffraction data which measures a single crystal; therefore the values obtained from single-crystal X-ray diffraction are considered to be more representative. According to the obtained structural formula, there is a significant amount of Si (0.234(2)) and Fe^{2+} (0.234(2)) on the octahedral position. This suggests that ~23 mol % of the endmember iron-majorite ($Fe_4Si_4O_{12}$) component is present in the synthesized skiagite-rich garnet.

Mössbauer spectroscopy and nuclear forward scattering

Skiagite-rich garnet crystals, identified using single crystal X-ray diffraction, were loaded into a DAC and studied at ambient pressure. We collected SMS spectra from a number of crystals and fit them to doublets with conventional constraints (equal doublet component widths and areas). All spectra gave hyperfine parameters that were the same within experimental uncertainty with the exception of relative intensities of the different doublets. This difference likely arises from varying ratios of different iron isotopes due to the starting mixture containing unenriched $Fe_{1-x}O$ and ^{57}Fe-enriched Fe_2O_3, where partial isotopic differentiation occurred in the course of the chemical reaction.

A typical SMS spectrum of skiagite-rich garnet contains two doublets (Fig. 2) that according to literature data (Amthauer et al. 1976; Woodland and Ross 1994) can be assigned to Fe^{2+} on the dodecahedral site and Fe^{3+} on the octahedral site. Some of the crystals showed an additional doublet consistent with Fe^{2+} on the octahedral site, although with low intensity

likely due to the isotopic effect mentioned above. The NFS spectrum collected at ambient conditions (Fig. 3) is consistent with the SMS spectrum and the fit gave similar hyperfine parameters (Table 5). Since the absolute CS value cannot be determined from the NFS data, it was fixed to the value determined from the SMS spectrum.

XANES

XANES spectra were simulated using *ab initio* multiple scattering calculations with the FEFF9 code (Rehr et al. 2009). The atomic clusters for Fe1 and Fe2 positions were calculated from the structural model obtained in the single-crystal X-ray diffraction study. Full multiple scattering calculations were performed in a 6 Å radius cluster, while self-consistent potentials were calculated for a 4 Å radius cluster. The Hedin-Lundqvist self-energy exchange correlation was used and multipole (dipole + quadrupole) transitions were calculated to simulate the pre-edge transition peak.

Figure 4 shows the experimental XANES spectra of skiagite-rich garnet and simulated XANES spectra for the adopted structural model. Energies of simulated spectra were shifted so as to fit each simulated curve to the corresponding observed spectra.

Each spectrum is characterized by two parts: a pre-edge region (~7113 eV) and a main-edge region (7120-7150 eV). Because skiagite-rich garnet is cubic, there is no linear polarization effect and spectra are the same for any crystal orientation. Our experimental setup at the beamline did not allow the collection of spectra with sufficient quality in the pre-edge region. However, comparison of the main-edge regions suggests that the simulated spectra are representative of the experimental ones.

Comparison of the crystal structures of Fe-bearing garnet endmembers

The most abundant endmembers of Fe-bearing garnets are almandine, $Fe^{2+}_3Al_2Si_3O_{12}$, and andradite, $Ca_3Fe^{3+}_2(SiO_4)_3$, which are stable at ambient pressure. Knorringite,

193 $Fe_3Cr_2Si_3O_{12,}$ is stable above 6 GPa (Fursenko 1981). Majorite, $Mg_3(Fe^{2+}Si)(SiO_4)_3$, is
194 considered to be an abundant garnet component at depths >350 km (Ringwood 1975). All of
195 the endmembers form solid solutions with skiagite (Fig. 5).

196 Woodland and Ross (1994) carried out a single-crystal X-ray diffraction study of two
197 almandine-skiagite and five andradite-skiagite crystals in order to investigate variations in
198 bond length with increasing skiagite content. In andradite-skiagite solid solutions Fe^{2+}
199 substitutes for the larger Ca^{2+} on the dodecahedral sites, so that an increase of the skiagite-
200 component leads to shortening of average $((Fe^{2+},Ca) - O)_1$ and $((Fe^{2+},Ca) - O)_2$ bond lengths.
201 Since six of the twelve octahedral edges are shared with neighboring dodecahedra, the
202 octahedral Fe-O bond lengths also shorten. In almandine-skiagite solid solutions an increase
203 of the skiagite-component means that Al^{3+} is substituted by larger Fe^{3+} cations on octahedral
204 sites that results in an increase of the cation-oxygen octahedral $(Fe^{3+},Al) - O)$ bond lengths,
205 whereas the lengths of the two non-equivalent dodecahedral bonds $(Fe - O)_1$ and $(Fe - O)_2$
206 remain almost constant (Fig. 6).

207 The tetrahedral (Si-O) bond lengths remain constant across all joins and undergo only
208 minor changes of ~0.005 Å in almandine-skiagite garnets and ~0.01 Å in andradite-skiagite
209 garnets. The change in Si-O bond lengths along the andradite-skiagite join is likely a response
210 to the large decrease in the volume of neighboring dodecahedra, which leads to a slight
211 distortion of tetrahedra.

212 *Majoritic component in synthetic garnets*

213 Iron majorite (Fe-maj, $Fe_4Si_4O_{12}$) is the hypothetical endmember of iron-bearing high-
214 pressure garnets. As demonstrated by Akaogi and Akimoto (1977), the solubility of iron
215 majorite in almandine reaches a maximum of 40 mol % between 9.0 and 10.0 GPa at 1000°C.
216 They estimated a unit-cell parameter of 11.595 Å (V = 1558.89 $Å^3$) for the $Fe^{2+}{}_4Si_4O_{12}$
217 endmember by extrapolation.

The solubility of the iron majorite component in skiagite has not been previously demonstrated. Woodland and O'Neill (1993) showed that no significant excess of silicon (>3 cations pfu) was detected in garnet synthesized at 10 GPa and 1100°C from a starting material with 60% skiagite and 40% majorite. This was confirmed by the observed cell parameter that did not deviate from that of pure skiagite (a = 11.7286 Å) (Woodland and O'Neill 1993).

The structural formula obtained from EMPA and single-crystal X-ray diffraction data shows that the skiagite-rich garnet synthesized in our experiment contains excess Si and Fe^{2+} entering the Y site. The cell parameter of this garnet is higher (a =11.7511 (2) Å) compared to the one (a =11.7286 Å) reported by Woodland and O'Neil (1993) for pure skiagite. This can be explained by incorporation of the iron majorite component (23 mol % $Fe_4Si_4O_{12}$) into skiagite due to the reaction $Fe^{2+}_3Fe^{3+}_2Si_3O_{12} = 2Fe^{2+}SiO_3 + Fe^{2+}Fe^{3+}_2O_4 + SiO_2$. Additionally, our structural data provide evidence for increase of the unit cell parameter from skiagite to iron majorite (dashed line in Fig. 7). If the data are linearly extrapolated (Fig. 7), the unit cell parameter of iron majorite in our study is found to be a = 11.833 Å, which is higher than the value obtained by Akaogi and Akimoto (1977) (a = 11.595 Å) through extrapolation of iron majorite – almandine solubility data.

Implications

The results of our study provide information on the solubility of the iron-majorite endmember in skiagite. We have demonstrated the possibility to synthesize high quality single crystals of majorite-skiagite garnet and through single-crystal X-ray diffraction data revealed that at least 23 mol % of iron-majorite can be dissolved in skiagite at high pressure and high temperature conditions. The studied garnet contains octahedral Si, which can be an important pressure indicator for garnets in mantle assemblages (Akaogi and Akimoto 1977). The relationship between skiagite and majorite provides evidence for similarity in their crystal chemical behavior, but, at the same time, suggests a consequent reaction on pressure increase.

Although both are high-pressure components of garnet, the proportion of iron majorite component relative to skiagite should decrease with increasing pressure. Our data motivates a detailed investigation of structural changes in the skiagite–majorite series as a function of pressure and temperature.

Acknowledgments

This study was partly supported by the Russian Foundation for Basic Research (project no. 15-05-08261 to Leyla Ismailova and Andrey Bobrov). We acknowledge the European Radiation Facility for provision of synchrotron radiation facilities (BM01 SNBL, ID18, ID24). We would like to thank U. Trenz and D. Krauße for support during the SEM and microprobe measurements.

255 ***References***

256 Akaogi, M., and Akimoto, A. (1977) Pyroxene-garnet solid-solution equilibria in the system
257 $Mg_4Si_4O_{12}$-$Mg_3Al_2Si_2O_{12}$ and $Fe_4S_{i4}O_{12}$- $Fe_3Al_2Si_3O_{12}$ at high pressures ant temperatures.
258 Physics of the Earth and Planetary Interiors, 111, 90-106.

259 Amthauer, G., Annersten, H., and Hafner, SS. (1976) The Mössbauer spectrum of ^{57}Fe in
260 silicate garnets. Z. Kristallogr 143: 14-55.

261 Armbuster, T., and Geiger, C.A. (1993) Andradite crystal chemistry, dynamic X-site disorder,
262 and structural strain in silicate garnets. European Journal of Mineralogy, 5, 59-71.

263 Armbuster, T., Geiger, C.A., and Lager, G.A. (1992) Single crystal X-ray structure study of
264 synthetic pyrope almandine garnets at 100 and 298 K. American Mineralogist ,77: 512-521.

265 Frost D.J., Poe B. T., Tronnes R. G., Liebske C., Duba A., and Rubie D.C. (2004) A new
266 large-volume multianvil system. Physics of the Earth and Planetary Interiors, 143-144, 507-
267 514.

268 Fursenko, B. A. (1981) Synthesis of new high pressure garnets: $Mn_3Cr_2Si_3O_{12}$ and
269 $Fe_3Cr_2Si_3O_{12}$. Bulletin de Minéralogie, 104, 418-422.

270 Gasparik, T. (1989) Transformation of enstatite – diopside – jadeite pyroxenes to garnet.
271 Contributions to Mineralogy and Petrology ,102, 389-405.

272 Irifune, T., (1987) An experimental investigation of the pyroxene-garnet transformation in a
273 pyrolite composition and its bearing on the constitution of the mantle. Physics of the Earth
274 and Planetary Interiors, 45, 324-336.

275 Karpinskaya T.B., Ostrovsky I.A., and Yevstigneeva, T.L. (1982) Synthetic pure iron skiagite
276 garnet. Izvestia Akademie Nauk, SSSR, 9, 128-129 (in Russian).

277 Novak, G.A., and Gibbs, G.V. (1971) The crystal chemistry of silicate garnets. American
278 Mineralogist, 56, 791-825.

279 Ono, S., and Yasuda, A. (1996). Compositional change of majoritic garnet in a MORB
280 composition from 7 to 17GPa and 1400 to 1600°C. Physics of the Earth and Planetary
281 Interiors, 96, 171-179.

282 Pascarelli, S., Mathon, O., Muñoz, M., Mairs, T., and Susini, J. (2006) Energy-dispersive
283 absorption spectroscopy for hard-X-ray micro-XAS applications. Journal of synchrotron
284 radiation, 13, 351–358.

285 Petricek,V., Dusek, M., and Palatinus, L. (2014) Crystallographic Computing System
286 JANA2006: General features. Zeitschrift für Kristallographie, 229, 345–352

287 Potapkin, V., Chumakov, A.I., Smirnov, G.V., Celse, J.-P., Rüffer, R., McCammon, C., and
288 Dubrovinsky, L. (2012) The ^{57}Fe synchrotron Mössbauer source at the ESRF. Journal of
289 Synchrotron Radiation, 19, 559-569.

290 Prescher, C., McCammon, C., and Dubrovinsky, L. (2012) MossA: a program for analyzing
291 energy-domain Mössbauer spectra from conventional and synchrotron sources. Journal of
292 Applied Crystallography, 45, 329-331.

293 Bunau, O., and Joly Y. (2009) Self-consistent aspects of x-ray absorption calculations.
294 Journal of Physics: Condensed Matter, 21, 345501

295 Rehr, J.J., Kas, J.J., Prange, M.P., Sorini, A.P., Takimoto, Y., and Vila, F. (2009) *Ab initio*
296 theory and calculations of X-ray spectra. Comptes Rendus Physique, 10 (6), 548-559.

297 Ringwood, A.E. (1975) Composition and petrology of the Earth's mantle, 618 p. McGraw
298 Hill, New York.

Rüffer, R., and Chumakov, A.I. (1996) Nuclear resonance beamline at ESRF. Hyperfine Interactions, 97-98, 589-604.

Stachel, T. (2001) Diamonds from the asthenosphere and the transition zone. European Journal of Mineralogy, 13(5), 883-892.

Woodland, A.B., and O'Neill, H.St.C. (1993) Synthesis and stability of $Fe_3^{2+}Fe_2^{3+}Si_3O_{12}$ garnet and phase relations with $Fe_3Al_2Si_3O_{12}$ – $Fe_3^{2+}Fe_2^{3+}Si_3O_{12}$ solutions. American Mineralogist , 78, 1000-1013.

Woodland, A.B., and Ross II, C.R. (1994) A crystallographic and Mössbauer spectroscopy study of $Fe_3Al_2Si_3O_{12}$ – $Fe_3^{2+}Fe_2^{3+}Si_3O_{12}$ and $Ca_3Fe_2^{3+}Si_3O_{12}$ - $Fe_3^{2+}Fe_2^{3+}Si_3O_{12}$ (andradite-skiagite) garnet solid solutions. Physic and Chemistry of Minerals, 21, 117-132.

Woodland, A.B., and O'Neill, H.St.C. (1995) Phase relations between $Ca_3Fe_2^{3+}Si_3O_{12}$ – $Fe_3^{2+}Fe_2^{3+}Si_3O_{12}$ garnet and $CaFe_2Si_2O_6$ – $Fe_2Si_2O_6$ pyroxene solid solutions. Contributions to Mineralogy and Petrology, 121, 87-98.

Woodland, A.B., Bauer M., Boffa Ballaran T., and Hanrahan M. (2009) Crystal chemistry of $Fe_3Cr_2Si_3O_{12}$ –$Fe_3Fe_2Si_3O_{12}$ garnet solid solutions and related spinels. American Mineralogist, 94, 359-366.

321

322

323 **Figure captions**

324 **Figure 1.** Back scattered electron image of the sample (S5962) synthesized at 9.5 GPa and
325 1100 ^{o}C consisting of skiagite-rich garnet (Ski- gray), clinopyroxene (Cpx- light gray), coesite
326 (Coe- black) and magnetite (Mag- white).

327 **Figure 2.** ^{57}Fe SMS spectrum of skiagite-rich garnet at ambient conditions. The solid line
328 shows the fit with parameters given in Table 5. Red and blue doublets represent Fe^{2+} and Fe^{3+},
329 respectively.

330 **Figure 3.** NFS spectrum of skiagite-rich garnet at ambient conditions. The solid line shows
331 the fit with parameters given in Table 5. The inset shows the energy domain spectrum
332 represented by the time domain data.

333 **Figure 4.** Normalised Fe K-edge XANES spectra (solid line – experimental and dashed line –
334 simulated) of skiagite-rich garnet at ambient conditions.

335 **Figure 5.** Unit cell volume, V, plotted as a function of the skiagite content in andradite-
336 skiagite, almandine-skiagite, and knorringite-skiagite solid solutions. Data for almandine-
337 skiagite and andradite-skiagite are from Woodland and Ross (1994), and for knorringite-
338 skiagite from Woodland et al. (2009). The open square indicates the skiagite-majorite solid
339 solution from this study. Uncertainties are less than the size of the symbols.

340 **Figure 6.** Variation of the X-O and Y-O bonds lengths with the proportion of skiagite-
341 component in andradite-skiagite and almandine-skiagite solid solutions (X and Y indicate
342 cations in dodecahedral (X) and octahedral (Y) sites) after Woodland and Ross (1994). Data
343 for the andradite (solid triangles) and almandine (opened triangles) endmembers are from
344 Armbruster et al. (1992) and Armbuster and Geiger (1993). Open squares indicate the
345 skiagite-majorite garnet from this study.

346

347

348

349 **Table 1** Crystal data and structure refinement

Chemical formula	$Fe^{2+}_3(Fe^{2+}_{0.234}Fe^{3+}_{1.532}Si_{0.234})\ Si_3\ O_{12}$
Formula weight (g/mol)	548.98
Crystal system, space group	Cubic, $Ia\bar{3}d$
Temperature (K)	280.0(1)
a (Å)	11.7511 (2)
V (Å^3)	1622.69 (5)
Z	8
Radiation type	Synchrotron, λ= 0.6946 Å
μ (mm^{-1})	10.997
Crystal size (mm)	0.02 × 0.019 × 0.01
Density (calculated)	4.494 g/cm^3
Data collection	
Absorption correction	Multi-scan (SCALE3 ABSPACK)
T_{min}, T_{max}	0.730, 1
No. of measured, independent and observed [$I > 3\sigma(I)$] reflections	5517, 255, 215
R_{int}	0.028
$(\sin\theta/\lambda)_{max}$ (Å^{-1})	0.763
Refinement	
$R_F[I>3\sigma(I)]$, $wR(all)$, S	0.028, 0.043, 2.33

No. of reflections	255
No. of parameters	18
$\Delta\rho_{max}$, $\Delta\rho_{min}$ (eÅ^{-3})	0.63, -0.69

350

351

Table 2 Fractional atomic coordinates and equivalent isotropic (U_{eq}) displacement parameters ($Å^2$)

	X	*Y*	*Z*	U_{eq}	Occupancy
Fe2	1/8	0	1/4	0.0122 (2)	
Fe1	0	0	0	0.0077 (2)	0.883 (7)
Si2	3/8	0	1/4	0.0085 (3)	
O1	0.03501 (15)	0.05281 (15)	0.65693 (15)	0.0112 (5)	
Si1	0	0	0	0.0077 (2)	0.117(7)

Table 3 Atomic displacement parameters (Å^2)

	U^{11}	U^{22}	U^{33}	U^{12}	U^{13}	U^{23}
Fe2	0.0081 (4)	0.0143 (3)	0.0143 (3)	0	0	0.0012 (3)
Fe1	0.0077 (4)	0.0077 (4)	0.0077 (4)	0.00007 (17)	0.00007 (17)	0.00007 (17)
Si2	0.0072 (6)	0.0092 (4)	0.0092 (4)	0	0	0
O1	0.0109 (8)	0.0126 (8)	0.0100 (8)	0.0010 (7)	−0.0007 (7)	−0.0001 (6)
Si1	0.0077 (4)	0.0077 (4)	0.0077 (4)	0.00007 (17)	0.00007 (17)	0.00007 (17)

Table 4 Selected geometric parameters: interatomic distances (Å), bond angles in degrees.

Fe2—Fe1	3.2845 (19)	Fe2—O1^{ii}	2.3831 (17)
Fe2—Si2	2.9378 (10)	Fe1—O1^{iii}	1.9888 (17)
Fe2—O1^{i}	2.2620 (18)	Si2—O1^{i}	1.6430 (18)
O1^{iv}—Fe2—O1^{i}	115.19 (6)	O1^{i}—Fe2—O1^{viii}	123.62 (6)
O1^{v}—Fe2—O1^{i}	71.69 (6)	O1^{i}—Fe2—O1^{ii}	73.03 (6)
O1^{v}—Fe2—O1^{ii}	111.13 (6)	O1^{viii}—Fe2—O1^{ii}	161.88 (6)
O1^{vi}—Fe2—O1^{i}	93.00 (6)	O1^{ix}—Fe1—O1^{iii}	91.89 (7)
O1^{vi}—Fe2—O1^{ii}	71.89 (6)	O1^{x}—Fe1—O1^{xi}	88.11 (7)
O1^{vii}—Fe2—O1^{i}	67.55 (6)	O1^{xi}—Fe1—O1^{iii}	180.0 (5)
O1^{vii}—Fe2—O1^{viii}	73.03 (6)	O1^{xii}—Si2—O1^{i}	114.47 (9)
O1^{vii}—Fe2—O1^{ii}	123.62 (6)	O1^{vii}—Si2—O1^{i}	99.87 (9)

Symmetry code(s):

(i) x+1/4, z-3/4, y+1/4;

(ii) -z+3/4, y-1/4, -x+1/4;

(iii) y, z-1/2, -x; (iv) -x, -y, -z+1;

(v) z-1/2, x, -y+1/2; (vi) z-1/2, -x, y;

(vii) x+1/4, -z+3/4, -y+1/4;

(viii) -z+3/4, -y+1/4, x+1/4;

(ix) x, -y, -z+1/2;

(x) -z+1/2, x, -y;

(xi) -y, -z+1/2, x;

(xii) -x+1/2, -y, z-1/2.

Table 5 Hyperfine parameters of skiagite-rich garnet at ambient conditions.

Oxidation state	Position	Center shift (CS)* [mm/s]	Quadrupole splitting (QS) [mm/s]	FWHM [mm/s]
SMS spectroscopy				
Fe^{2+}	Dodecahedral	1.31(1)	3.45(2)	0.15(3)
Fe^{3+}	Octahedral	0.37(1)	0.26(2)	0.19(4)
NFS spectroscopy				
Fe^{2+}	Dodecahedral	1.31**	3.49(5)	
Fe^{3+}	Octahedral	0.40(5)	0.27(1)	

*relative to α-Fe

**fixed to value from SMS

Coe

Ski

Cpx

Mag

10 µm

EHT = 20.00 kV

WD = 24.9 mm

Mag = 717 X

Photo No. = 197

Signal A = RBSD

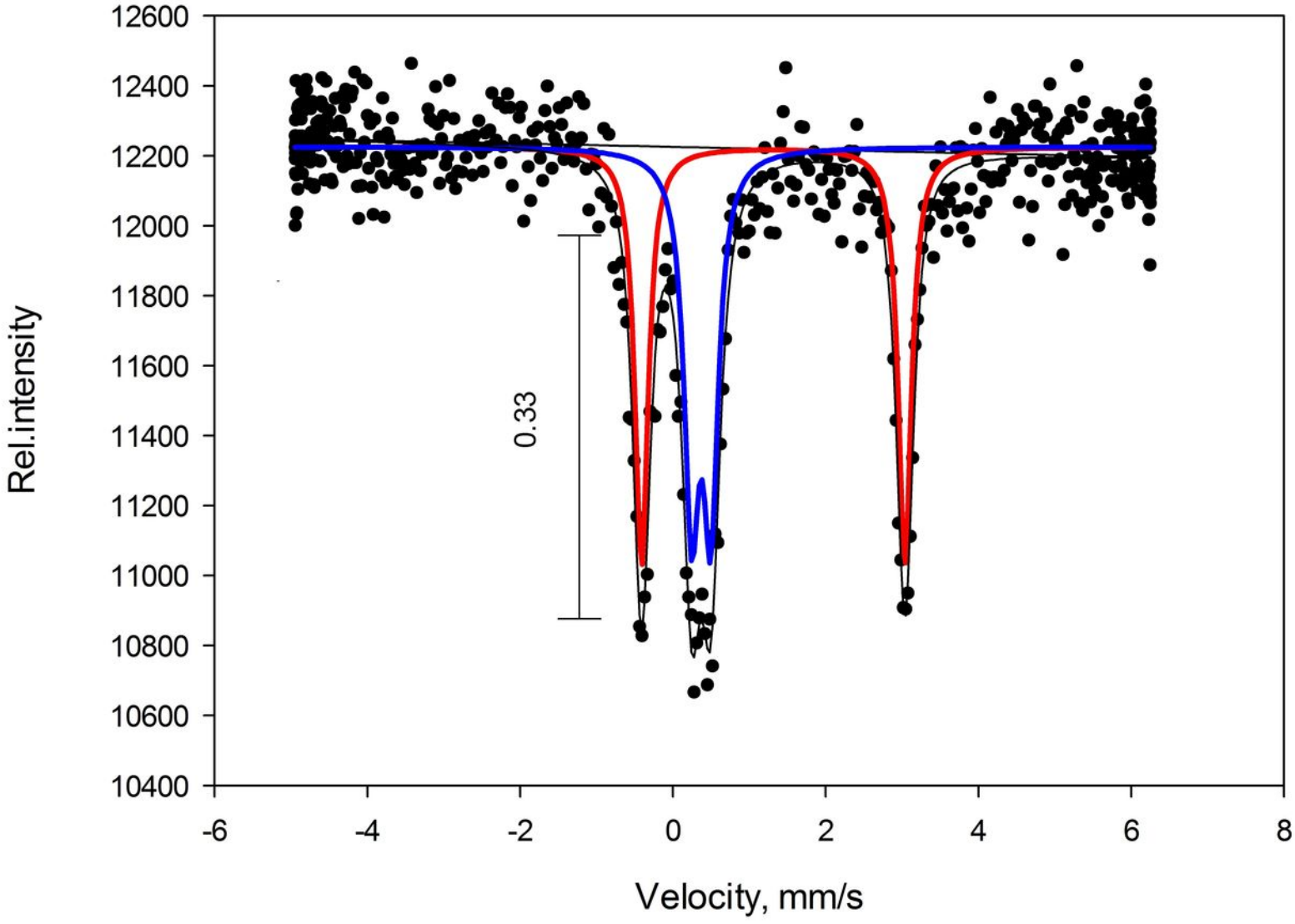
12600
12400
12200
12000
11800
11600
11400
11200
11000
10800
10600
10400
Rel.intensity
0.33
-6
-4
-2
0
2
4
6
8
Velocity, mm/s

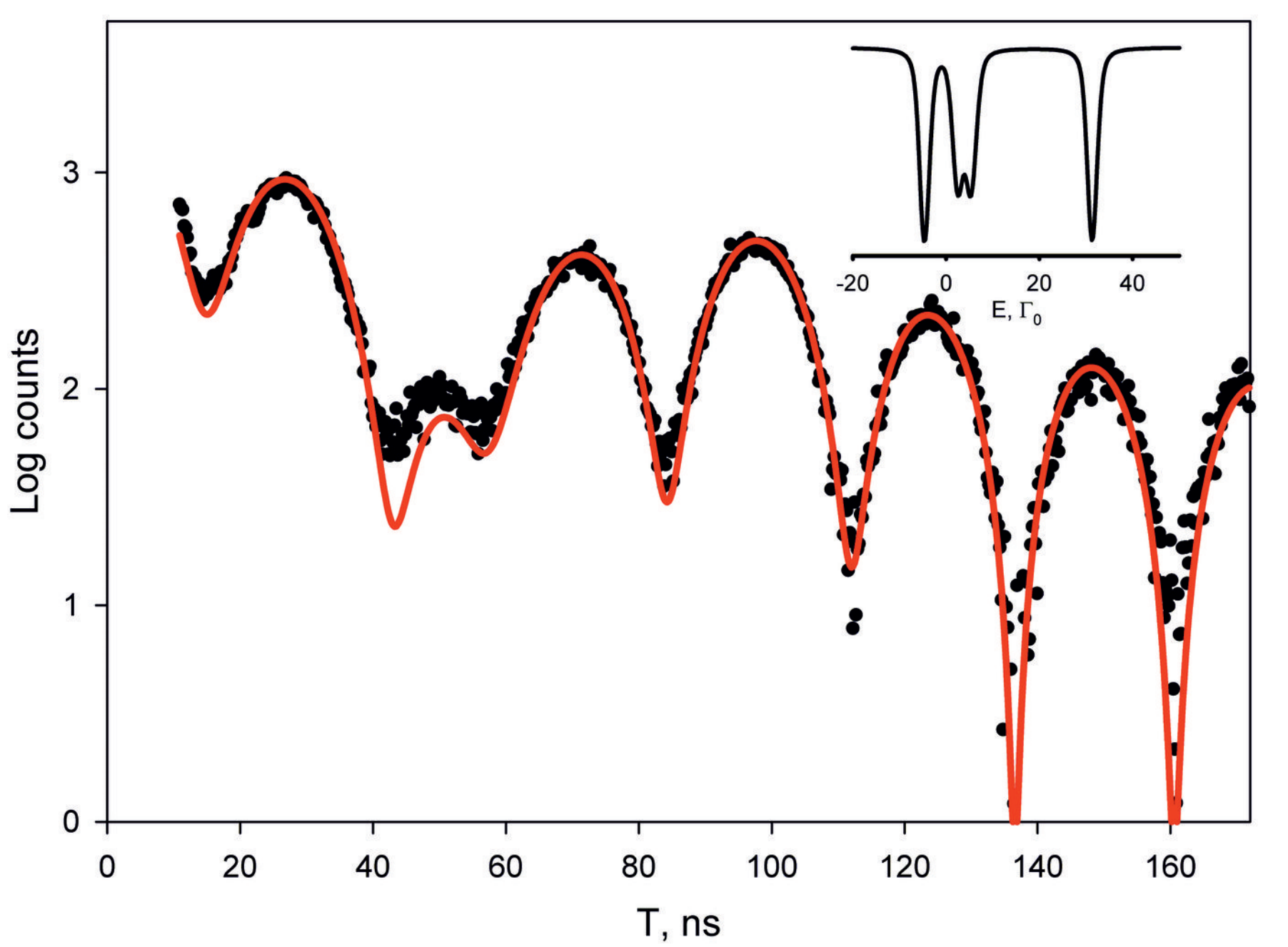
Log counts
T, ns
0
1
2
3
0
20
40
60
80
100
120
140
160
-20
0
20
40
E, Γ0

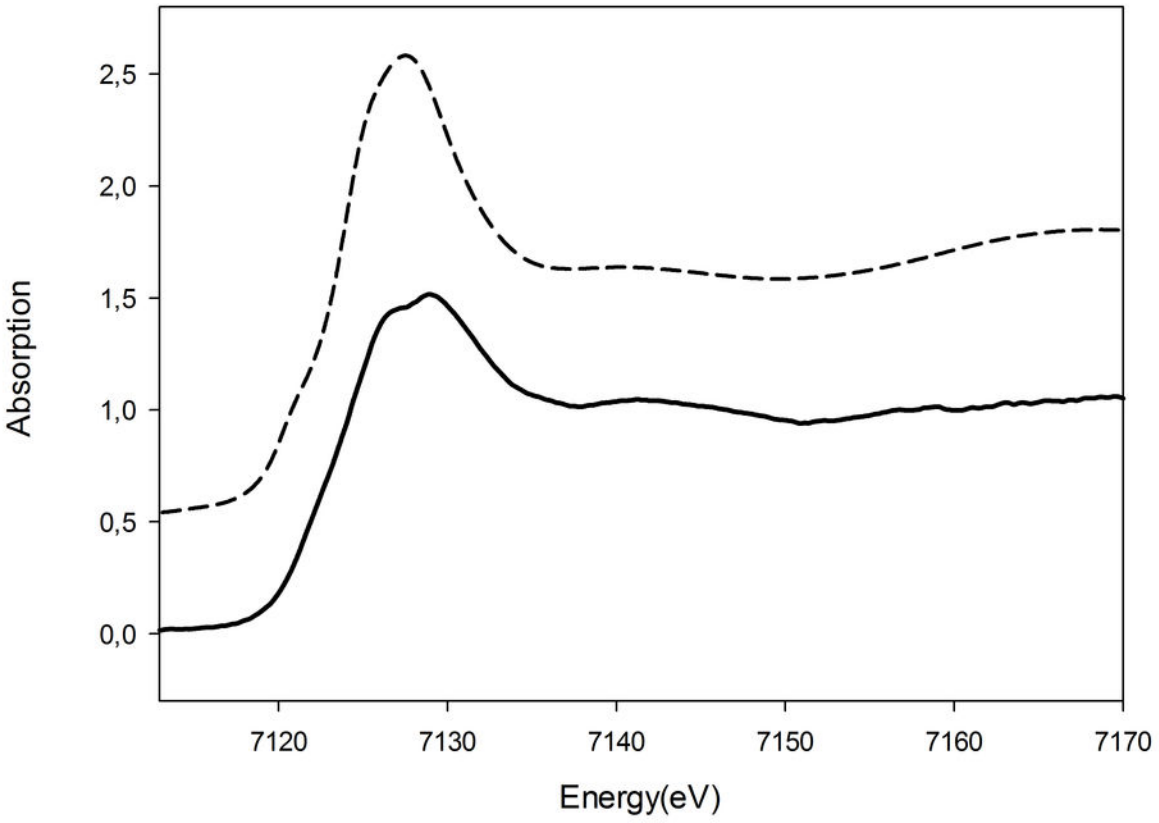
Absorption
2,5
2,0
1,5
1,0
0,5
0,0
7120
7130
7140
7150
7160
7170
Energy(eV)

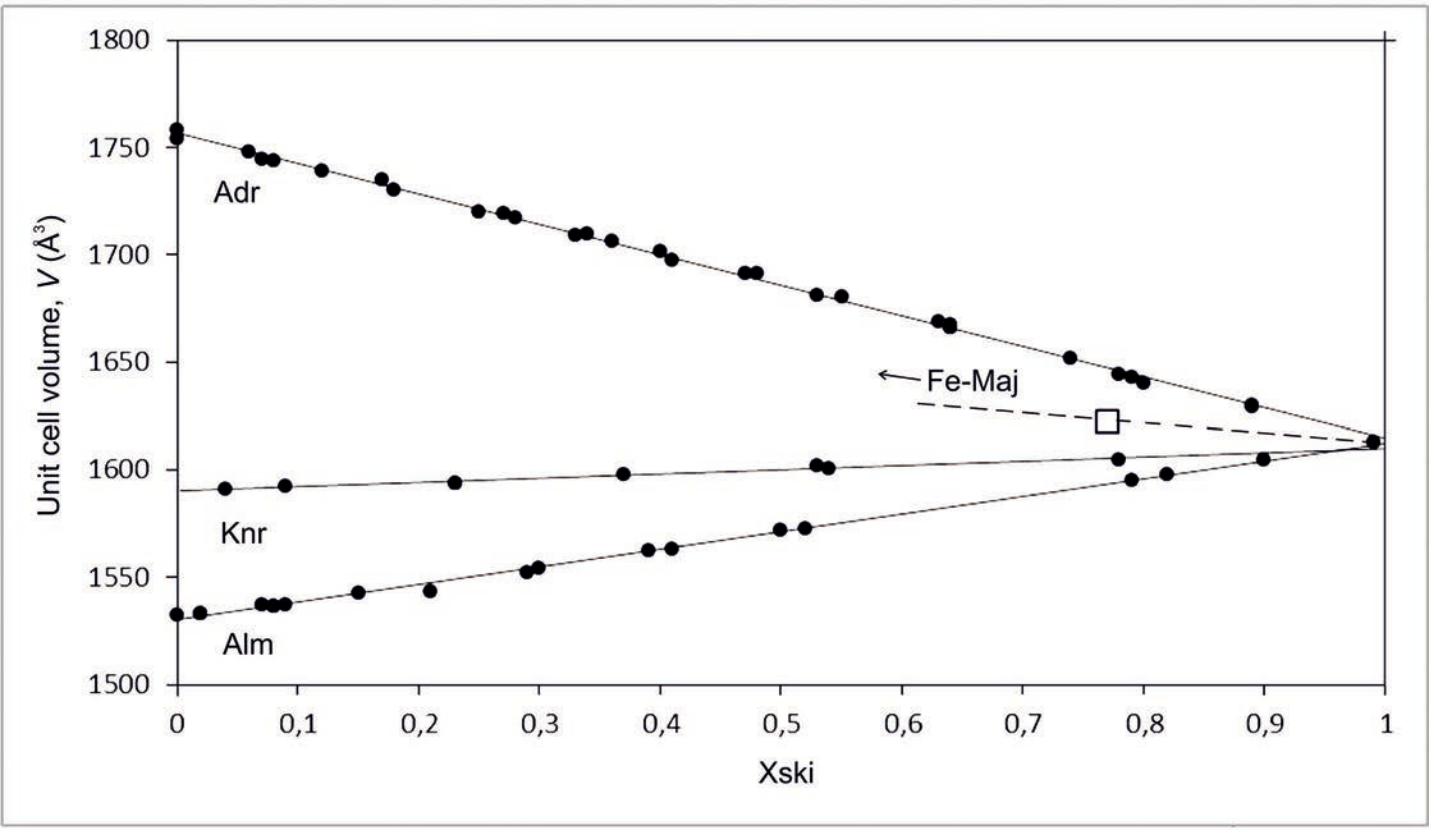
1800
1750
1700
1650
1600
1550
1500
Unit cell volume, V (Å3)
Adr
Fe-Maj
Knr
Alm
0
0,1
0,2
0,3
0,4
0,5
0,6
0,7
0,8
0,9
1
Xski

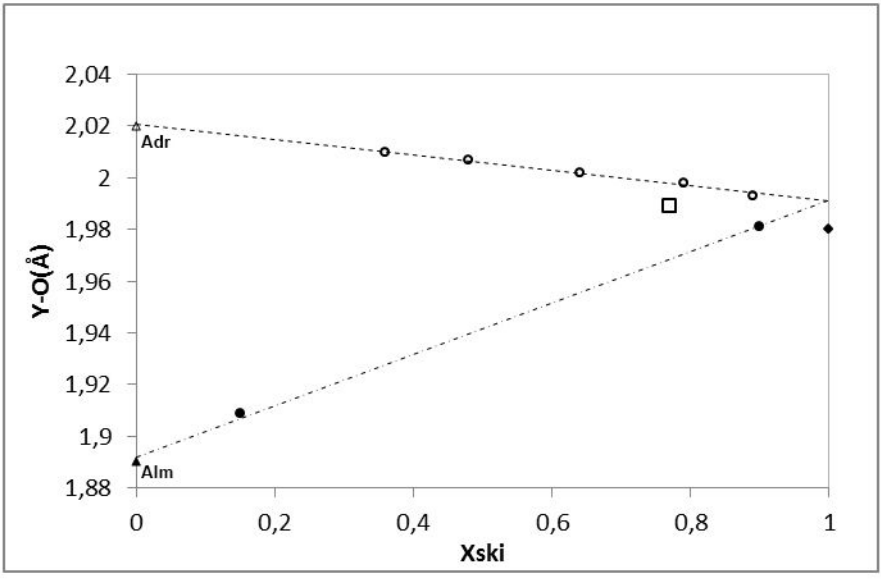
2,04
2,02
2
1,98
1,96
1,94
1,92
1,9
1,88
Y-O(Å)
Adr
Alm
0
0,2
0,4
0,6
0,8
1
Xski

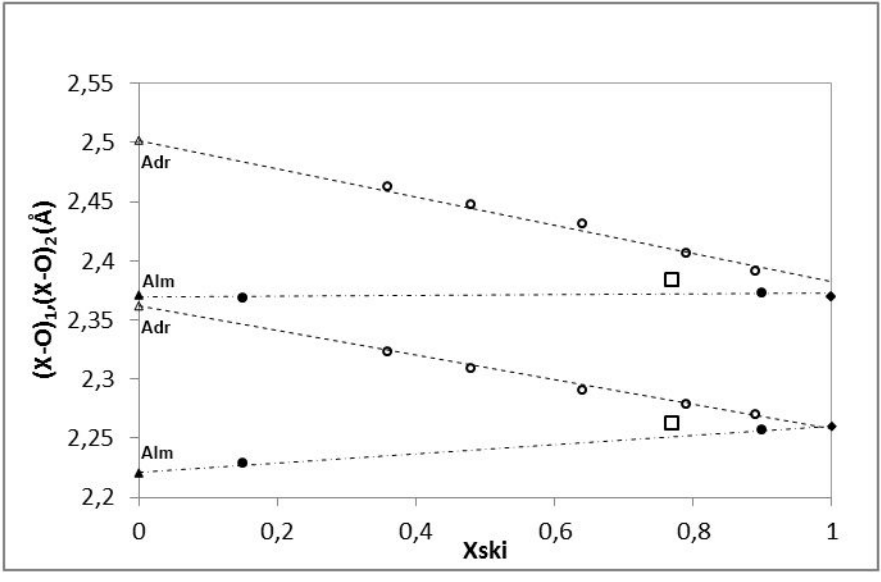
2,55
2,5
2,45
2,4
2,35
2,3
2,25
2,2
(X-O)1,(X-O)2(Å)
Adr
Alm
Adr
Alm
0
0,2
0,4
0,6
0,8
1
Xski